FUZZY LOGIC CONTROL OF A DUAL-STATOR INDUCTION GENERATOR FOR WIND ENERGY CONVERSION SYSTEMS

Hocine AMIMEUR Farid HAMOUDI
Laboratoire de Maitrise des Energies Renouvelables (LMER)
Faculté de Technologie, Université de Bejaia, 06000 Bejaia, Algeria
hocine.amimeur@univ-bejaia.dz, f_hamoudi@yahoo.fr

Abstract: *This paper presents a fuzzy logic control (FLC) associated to the indirect field oriented control (IFOC) of a dual-stator induction generator (DSIG) based wind energy conversion systems (WECS). The DSIG has two sets of stator three-phase windings spatially shifted by 30 electrical degrees. The study of operation of the wind turbine leads us to two essential cases: optimization of the power for wind speeds lower than the nominal speed of the turbine and limitation of the power for higher speeds. Conventional electrical grid connected WECS present interesting control demands, due to the intrinsic nonlinear characteristic of wind mills and electric generators. The FLC has recently proved to be a successful control approach for complex nonlinear systems. The speed in the system is controlled by a fuzzy logic controller. In order to verify the validity of the proposed method, a dynamic model of the proposed system has been simulated, to demonstrate its performance.*

Key words: *Fuzzy logic control, dual-stator induction generator, indirect field-oriented control, winds energy conversion system.*

1. Introduction

The use of the wind energy conversion systems has been significantly expanded over the last few decades. This is due to the fact that this energy source production of electricity is emission free. Therefore, the study of induction generator has regained importance. The primary advantages of induction generator are less maintenance cost, better transient performance, without dc power supply for field excitation, brushless construction (squirrel-cage rotor), etc. [1].

The power rating of an ac drive system can be increased by using multiphase drives system which has more than three phases in the stator of the machine. Multiphase drives system possess several advantages over conventional three-phase drives, such as reducing the amplitude and increasing the frequency of the torque pulsation, reducing the rotor harmonic currents, reducing the current per phase without increasing the voltage per phase, lowering the dc-link current harmonics, power segmentation and high reliability. For this reason, multiphase induction machine drives are mainly related to the high-power and/or high-current applications such as for example in electric ship propulsion, in locomotive traction, in aerospace applications and electric / hybrid vehicles, etc. [1-3].

A very interesting and discussed in the literature multiphase solution is the dual-stator induction machine (DSIM) having two sets of three-phase windings spatially shifted by 30 electrical degrees with isolated neutral points.

Modeling, control and performance of dual stator (double star, dual three-phase) induction machine are extensively covered in [4-15].

The fuzzy set theory was introduced by L. A. Zadeh in 1965 [16]. The first FLC system is developed by E.H. Mamdani and S. Assilian, where control of a small steam engine is considered [17]. Thereafter, the applicability and success of FLC technique has been demonstrated in numerous practical control problems. Since the excellent robustness and adaptability are the best advantages of a FLC, it has been widely employed to control linear or nonlinear system. These advantages justify the necessity of applying this kind for the DSIG used in WECS.

Depending on the values of the average (steady state) wind speed, four zones may be identified in the static operation of WECS. Zones I and VI, where the provided power is zero, are not concerned by this paper. The interest is here focused on zone II, called partial load zone, where the extracted power proportionally depends of the wind speed cubed, and the so call load zone (III), where the power must be limited to the nominal value.

This paper is organized as follows. Modeling of the wind generator (modeling of the wind turbine and gearbox, description and modeling of the DSIG) and the maximum power point tracking (MPPT) algorithm to maximize the generated power are provided in Section 2. The indirect field oriented control (IFOC) of a DSIM is developed in Section 3. The fuzzy speed control is presented in Section 4. The grid side power control is developed in section 5. Finally, the system shown in Fig. 1 is used for numerical simulation and the related results are presented.

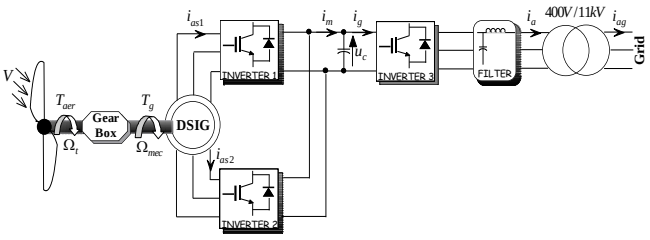

Fig. 1. Scheme of the studied device.

2. Modeling of the wind generator

2.1. Modeling of the wind turbine and gearbox

The aerodynamic power, which is converted by a wind turbine, is dependent on the power coefficient C_p. It is given by

$$P_t = \frac{1}{2} C_p(\lambda) \rho \pi R^2 V^3 \tag{1}$$

The turbine torque is the ratio of the output power to the shaft speed Ω_t, $T_{aer} = P_t / \Omega_t$.

The turbine is normally coupled to the generator shaft through a gearbox whose gear ratio G is chosen in order to set the generator shaft speed within a desired speed range. Neglecting the transmission losses, the torque and shaft speed of the wind turbine, referred to the generator side of the gearbox, are given by

$$T_g = \frac{T_{aer}}{G} \text{ and } \Omega_t = \frac{\Omega_{mec}}{G} \tag{2}$$

A wind turbine can only convert just a certain percentage of the captured wind power. This percentage is represented by $C_p(\lambda)$ which is function of the wind speed, the turbine speed and the pith angle of specific wind turbine blades [18].

Although this equation seems simple, C_p is dependent on the ratio λ between the turbine angular velocity and the wind speed V. This ratio is called the tip speed ratio

$$\lambda = \frac{\Omega_t R}{V} \tag{3}$$

A typical relationship between C_p and λ is shown in Fig. 2. It is clear from this figure that there is a value of λ for which C_p is maximum and that maximize the power for a given wind speed. The peak power for each wind speed occurs at the point where C_p is maximized. To maximize the generated power, it is therefore desirable for the generator to have a power characteristic that will follow the maximum C_{p_max} line.

If the wind speed is measured and the mechanical characteristics of the wind turbine are known, it is possible to deduce in real-time the optimal mechanical power which can be generated using the maximum power point tracking (MPPT). The optimal mechanical power can be expressed as

$$P_{mec\_opt} = -\frac{C_{p\_\max}}{\lambda^3_{C_{p\_\max}}} \cdot \frac{\rho \pi R^5}{2} \cdot \frac{\Omega^3_{mec}}{G^3} \tag{4}$$

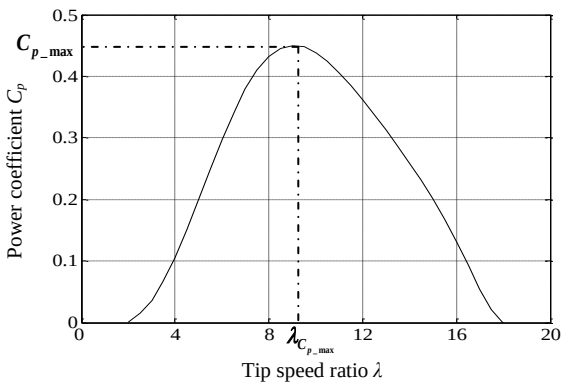

Fig. 2. Power coefficient for the wind turbine model.

2.2. Modeling of the DSIG

A schematic of the stator and rotor windings for a dual-stator induction machine is given in Fig. 3. The six stator phases are divided into two wye-connected three-phase sets, labeled (a_{s1}, b_{s1} and c_{s1}) and (a_{s2}, b_{s2} and c_{s2}), whose magnetic axes are displaced by α=30° electrical angle. The windings of each three-phase set are uniformly distributed and have axes that are displaced 120° apart. The three-phase rotor windings (a_r, b_r and c_r) are also sinusoidally distributed and have axes that are displaced by 120° apart.

The electrical equations of the dual-stator induction machine in the synchronous reference frame (d-q) are this given by [19-20]

$$v_{d1} = r_1 i_{d1} + p\psi_{d1} - \omega_e \psi_{q1} \tag{5}$$

$$v_{q1} = r_1 i_{q1} + p\psi_{q1} + \omega_e \psi_{d1} \tag{6}$$

$$v_{d2} = r_2 i_{d2} + p\psi_{d2} - \omega_e \psi_{q2} \tag{7}$$

$$v_{q2} = r_2 i_{q2} + p\psi_{q2} + \omega_e \psi_{d2} \tag{8}$$

$$v_{dr} = r_r i_{dr} + p\psi_{dr} - (\omega_e - \omega_r)\psi_{qr} = 0 \tag{9}$$

$$v_{qr} = r_r i_{qr} + p\psi_{qr} + (\omega_e - \omega_r)\psi_{dr} = 0 \tag{10}$$

The expressions for stator and rotor flux linkages are

$$\psi_{d1} = L_1 i_{d1} + L_m (i_{d1} + i_{d2} + i_{dr}) \tag{11}$$

$$\psi_{q1} = L_1 i_{q1} + L_m (i_{q1} + i_{q2} + i_{qr}) \tag{12}$$

$$\psi_{d2} = L_2 i_{d2} + L_m (i_{d1} + i_{d2} + i_{dr}) \tag{13}$$

$$\psi_{q2} = L_2 i_{q2} + L_m (i_{q1} + i_{q2} + i_{qr}) \tag{14}$$

$$\psi_{dr} = L_r i_{dr} + L_m (i_{d1} + i_{d2} + i_{dr}) \tag{15}$$

$$\psi_{qr} = L_r i_{qr} + L_m (i_{q1} + i_{q2} + i_{qr}) \tag{16}$$

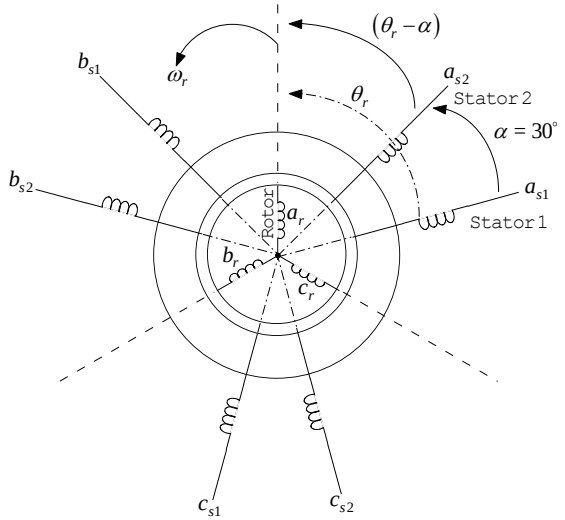

Fig. 3. Scheme of dual-stator winding induction machine.

The electromagnetic torque is evaluated as

$$T_{em} = \frac{PL_m}{(L_m + L_r)}\left[\left(i_{q1} + i_{q2}\right)\psi_{dr} - \left(i_{d1} + i_{d2}\right)\psi_{qr}\right] \quad (17)$$

The mechanical equation of machine is described as

$$Jp\Omega_{mec} + f\Omega_{mec} = T_{em} - T_g \quad (18)$$

The active and reactive power at the stator as well as those provide for grid are defined as

$$\begin{cases} P_1 = v_{d1}\, i_{d1} + v_{q1}\, i_{q1} \\ Q_1 = v_{q1}\, i_{d1} - v_{d1}\, i_{q1} \end{cases} \quad (19)$$

$$\begin{cases} P_2 = v_{d2}\, i_{d2} + v_{q2}\, i_{q2} \\ Q_2 = v_{q2}\, i_{d2} - v_{d2}\, i_{q2} \end{cases} \quad (20)$$

$$\begin{cases} P_s = P_1 + P_2 \\ Q_s = Q_1 + Q_2 \end{cases} \quad (21)$$

3. Indirect field oriented control of a DSIM

The main objective of the vector control of induction machines is, as in DC machines, to independently control the torque and the flux. In this order, one proposes to study the IFOC of the DSIM. The control strategy used consists to maintain the quadrate component of the flux null ($\psi_{qr} = 0$) and the direct flux equals to the reference ($\psi_{dr} = \psi_r^*$):

$$\psi_{dr} = \psi_r^* \quad (22)$$

$$\psi_{qr} = 0 \quad (23)$$

$$p\psi_r^* = 0 \quad (24)$$

Substituting (22), (23) and (24) into (9) and (10), yields

$$r_r i_{dr} + p\psi_r^* = 0 \Rightarrow i_{dr} = 0 \quad (25)$$

$$r_r i_{qr} + \omega_{sl}^* \psi_r^* = 0 \Rightarrow i_{qr} = -\frac{\omega_{sl}^* \psi_r^*}{r_r} \quad (26)$$

With $\omega_{sl}^* = \omega_e^* - \omega_r$, ($\omega_{sl}$ is the slip speed).

The rotor currents in terms of the stator currents are divided from (15) and (16) as

$$i_{dr} = \frac{1}{\left(L_m + L_r\right)}\left[\psi_r^* - L_m\left(i_{d1} + i_{d2}\right)\right] \quad (27)$$

$$i_{qr} = -\frac{L_m}{\left(L_m + L_r\right)}\left(i_{q1} + i_{q2}\right) \quad (28)$$

Substituting (28) into (26), obtain

$$\omega_{sl}^* = \frac{r_r L_m}{\left(L_m + L_r\right)}\frac{\left(i_{q1} + i_{q2}\right)}{\psi_r^*} \quad (29)$$

The final expression of the electromagnetic torque is

$$T_{em}^* = P\frac{L_m}{(L_m + L_r)}\left(i_{q1} + i_{q2}\right)\psi_r^* \quad (30)$$

With taking into the rotor field orientation, the stator voltage equations (5)-(8) can be rewritten as

$$v_{d1}^* = r_1 i_{d1} + L_1 p i_{d1} - \omega_e^*\left(L_1 i_{q1} + \tau_r \psi_r^* \omega_{sl}^*\right) \quad (31)$$

$$v_{q1}^* = r_1 i_{q1} + L_1 p i_{q1} + \omega_e^*\left(L_1 i_{d1} + \psi_r^*\right) \quad (32)$$

$$v_{d2}^* = r_2 i_{d2} + L_2 p i_{d2} - \omega_e^*\left(L_2 i_{q2} + \tau_r \psi_r^* \omega_{sl}^*\right) \quad (33)$$

$$v_{q2}^* = r_2 i_{q2} + L_2 p i_{q2} + \omega_e^*\left(L_2 i_{d2} + \psi_r^*\right) \quad (34)$$

Where $\tau_r = L_r / r_r$.

Consequently, the electrical and mechanical equations for the system after these transformations in the space control may be written as follows

$$p i_{d1} = \frac{1}{L_1}\left\{v_{d1}^* - r_1 i_{d1} + \omega_e^*\left(L_1 i_{q1} + \tau_r \psi_r^* \omega_{sl}^*\right)\right\} \quad (35)$$

$$p i_{q1} = \frac{1}{L_1}\left\{v_{q1}^* - r_1 i_{q1} - \omega_e^*\left(L_1 i_{d1} + \psi_r^*\right)\right\} \quad (36)$$

$$p i_{d2} = \frac{1}{L_2}\left\{v_{d2}^* - r_2 i_{d2} + \omega_e^*\left(L_2 i_{q2} + \tau_r \psi_r^* \omega_{sl}^*\right)\right\} \quad (37)$$

$$p i_{q2} = \frac{1}{L_2}\left\{v_{q2}^* - r_2 i_{q2} - \omega_e^*\left(L_2 i_{d2} + \psi_r^*\right)\right\} \quad (38)$$

$$p\psi_r = -\frac{r_r}{(L_r + L_m)}\psi_r + \frac{r_r L_m}{(L_r + L_m)}\left(i_{d1} + i_{d2}\right) \quad (39)$$

$$p\Omega_{mec} = \frac{1}{J}\left\{\frac{PL_m\left(i_{q1} + i_{q2}\right)\psi_r^*}{(L_m + L_r)} - T_g - f\Omega_{mec}\right\} \quad (40)$$

4. Fuzzy speed control

The proposed control scheme is a cascade structure at is shown in Fig. 4, in which five loops are required. The internal loops allow the control stator current components (i_{d1}, i_{d2}, i_{q1} and i_{q2}, based on conventional PI controllers), whereas the external loop provide the regulation of the mechanical speed (Ω_{mec}, based on fuzzy logic controller). The bloc diagram of the IFOC is presented in Fig. 5.

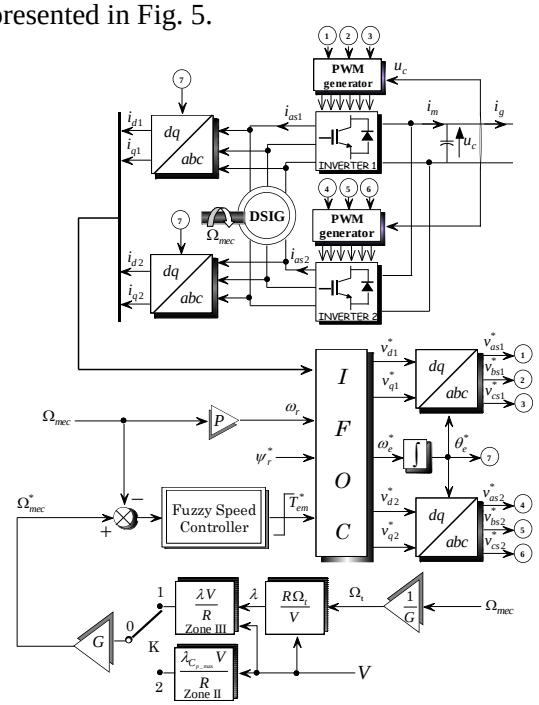

Fig. 4. IFOC associated fuzzy speed control scheme for DSIG in WECS.

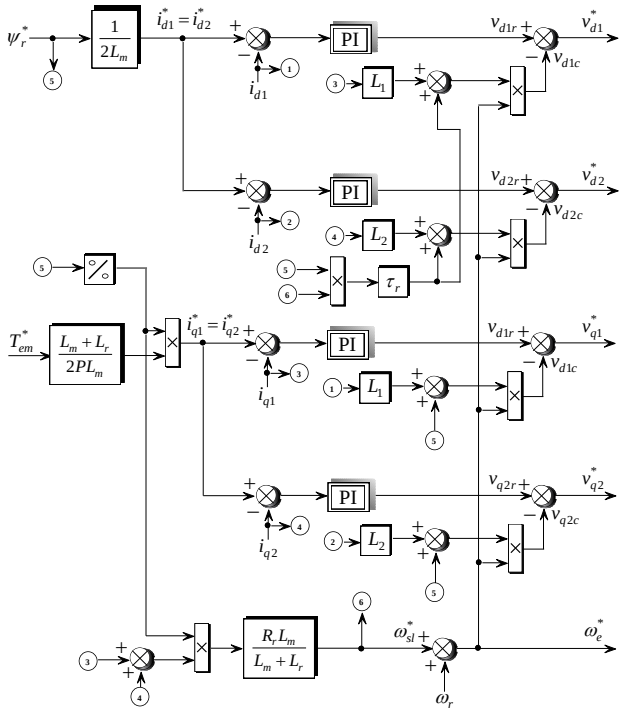

Fig. 5. Bloc diagram of the IFOC (based on conventional PI controllers).

The structure of a fuzzy speed controller is illustrated in Fig.6 is made up of the following elements

4.1. Scaling factors

The FLC inputs are the mechanical speed error (E) and change in mechanical speed error (dE/dt or CE for the sampling interval). The mechanical speed error is defined by

$$E = \Omega^*_{mec} - \Omega_{mec} \tag{41}$$

The chosen input scaling factors G_E and G_{CE} indicate the normalized values of error (E) and change in error (CE), i.e., G_E and G_{CE} are mapped onto the universe of discourse [-1, 1]. Similarly, the normalized output value is mapped into the physical domain by defuzzification and the output scaling factor G_U. The output scaling factor is a very important parameter of the FLC [21].

The relationship between the scaling factors and the inputs and output variables of the FLC are as follows:

$$e = G_E E \tag{42}$$

$$ce = G_{CE} CE \tag{43}$$

$$dU = G_U du \tag{44}$$

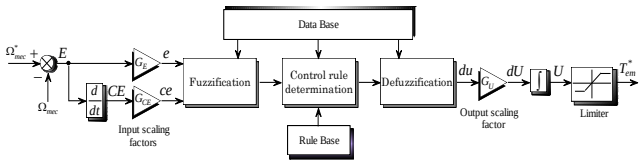

Fig. 6. Structure of the fuzzy speed controller.

4.2. Fuzzification

The fuzzification converts the real values into linguistic variables with assigning to each variable a set of fuzzy subsets. Among a set of membership functions, left-triangle, triangle and right-triangle membership functions are used for the inputs (e and ce) and output (du) as illustrated in Fig. 7. The linguistic variables of inputs and output are: NB (Negative Big), NM (Negative Medium), NS (Negative Small), Z (Zero), PS (Positive Small), PM (Positive Medium) and PB (Positive Big).

4.3. Control rule determination

The rule base of the speed controller determination is expressed as: IF (conditions) THEN (action) rules, for example: IF the error (e) is NS AND change in error (ce) is PB THEN the control increment (du) is PM. A 49 (7×7) rules of the FLC are given in matrix form in Table 1. The Mamdani's Max-Min inference method is used.

4.4. Defuzzification

In this stage the fuzzy variables are converted into a crisp variable. Defuzzification for this system is the centre of gravity to compute the output of this FLC

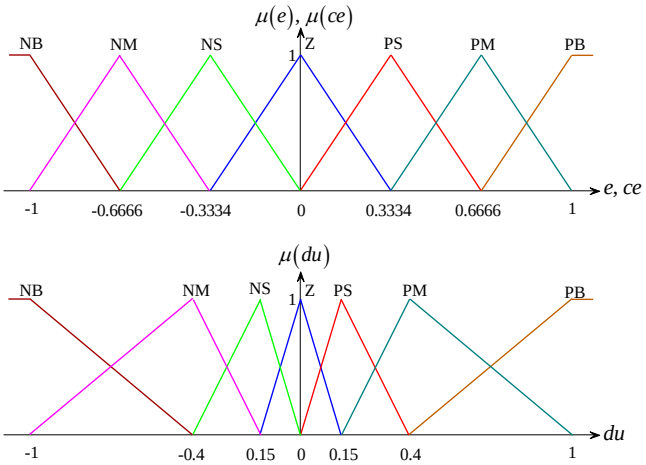

Fig. 7. Fuzzy logic membership functions for inputs (e and ce) and output (du) variables.

Table 1
Fuzzy rule table

du		de						
		PB	NM	NS	Z	PS	PM	PB
e	NB	NB	NB	NB	NB	NM	NS	Z
	NM	NB	NB	NB	NM	NS	Z	PS
	NS	NB	NB	NM	NS	Z	PS	PM
	Z	NB	NM	NS	Z	PS	PM	PB
	PS	NM	NS	Z	PS	PM	PB	PB
	PM	NS	Z	PS	PM	PB	PB	PB
	PB	Z	PS	PM	PB	PB	PB	PB

(*du*). The centre of gravity method is both very simple and very fast method. The output function is given as:

$$du = \frac{\sum_{i=1}^{n} \mu(du_i)\, du_i}{\sum_{i=1}^{n} \mu(du_i)} \tag{45}$$

Where, *n* is the total number of rules (49 rules) and $\mu(du_i)$ denotes the output membership value for i^{th} rule.

Finally, the output *dU (dU = G_U du)* is integrated to get the electromagnetic torque reference.

5. Grid side power control

In grid-connected control mode, all the available power that can be extracted from the wind generator is transferred to the grid. Standard PI controllers are used to regulate the dc link voltage and the inverter output currents in the (*abc*) synchronous frame. To have the grid current vector in phase with the grid voltage vector, the reference reactive power Q^* should be zero. The dc link voltage control is acting to supply the reference active power. The output of the current controllers sets the voltage reference for an average conversion control method that controls the switches of the grid inverter [22].

The dc link voltage is governed by

$$\frac{du_c}{dt} = \frac{1}{C}\left(i_m - i_g\right) \tag{46}$$

The reference active power injected to the electrical supply network is given by

$$P^* = u_c\left(i_m - i_c^*\right) = P_{dc\_m} - P_{dc}^* \tag{47}$$

Where, $i_c^* = \mathrm{PI}\left(u_c^* - u_c\right)$

To maintain constant the dc link voltage, we have recourse to use a proportional integral corrector. It is parameterized according to the capacitor value and the dynamics of the regulation loop.

Network reference currents, expressed in *d–q* frame, are given by

$$\begin{bmatrix} i_{id}^* \\ i_{iq}^* \end{bmatrix} = \frac{1}{v_{d\_mes}^2 + v_{q\_mes}^2} \begin{bmatrix} P^* & Q^* \\ -Q^* & P^* \end{bmatrix} \begin{bmatrix} v_{d\_mes} \\ v_{q\_mes} \end{bmatrix} \tag{48}$$

The reference voltages are obtained by

$$\begin{cases} v_{md}^* = v_d^* + v_{d\_mes} - \omega_e L_f i_{tq\_mes} \\ v_{mq}^* = v_q^* + v_{q\_mes} + \omega_e L_f i_{td\_mes} \end{cases} \tag{49}$$

With, $\begin{cases} v_d^* = \mathrm{PI}\left(i_{td}^* - i_{td\_mes}\right) \\ v_q^* = \mathrm{PI}\left(i_{tq}^* - i_{tq\_mes}\right) \end{cases}$

The control block of the grid connection conditioning system is shown in Fig. 8.

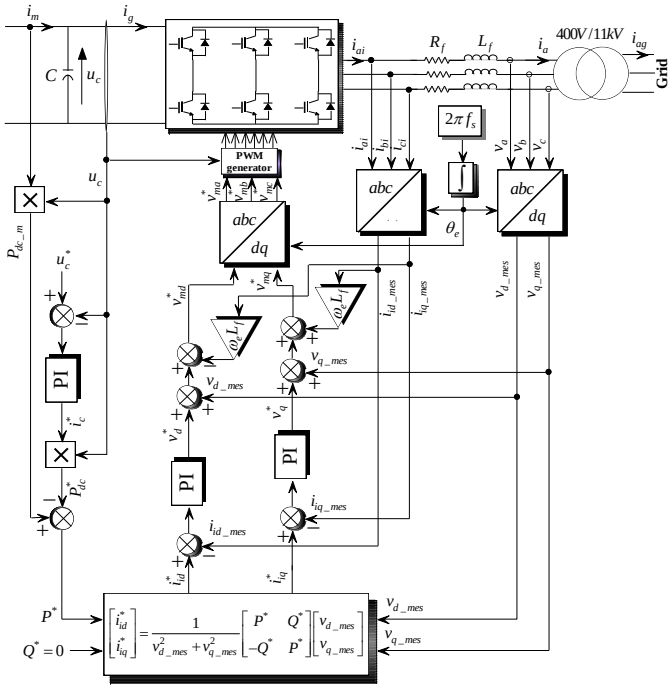

Fig. 8. Control bloc diagram of the grid connection conditioning system.

6. Simulation results and discussion

The dual-stator induction generator parameters used in the simulation are given in the Appendix B.

Whole the inverters (1)-(3) are modeled in the same way. The switches are considered as ideal, and their states are given by logical functions that take 1 the component is closed and 0 when it is open.

The results of simulations are obtained for reactive power $Q^* = 0$ and DC link voltage $u_c^* = 1130$V.

Fig. 9 shows the angular speed random of the DSIG. Fig. 10 presents the wind generator mechanical power. Fig. 11 shows the waveform of the generator torque. The decoupling effect of the between the direct and quadratic rotor flux of the DSIG is illustrated in Fig. 12. The stator currents and voltages waveforms of the DSIG and the related expended plots are shown, respectively, in Figs. 13a and 13b (phase a_{s1}).The PWM inverters are operated at 3,15kHz; hence, the currents are almost sinusoidal. The stator currents (winding set I and II) waveforms and these zoom are presented, correspondingly, in Figs. 14a and 14b. Fig. 15 gives the rotor current of the DSIG. The stator active and reactive powers are plotted in Fig. 16. Fig. 17 shows the regulation of the DC link voltage. It is maintained at a constant level (1130V) so that the real power extracted from the WECS can pass through the grid. The current and voltage at the output of the inverter 3 waveforms and these zoom are given, respectively, in Figs. 18a and 18b. The inverter 3 input

current is almost sinusoidal and at unity power factor. It is clear that the phase difference between the supply current and voltage is 180°, therefore the line side converter (rectifier) supplies real power to the utility grid. Fig. 19, in turn, gives the grid active and reactive powers. Finally, the grid current and voltage (phase *a*) and the related expended plots are shown, in that order, in Figs. 20a and 20b.

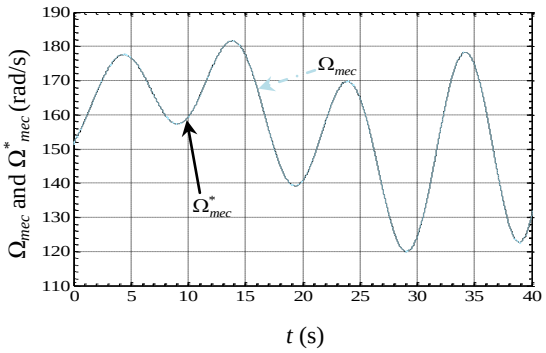

Fig. 9. Random of the DSIG rotor speed.

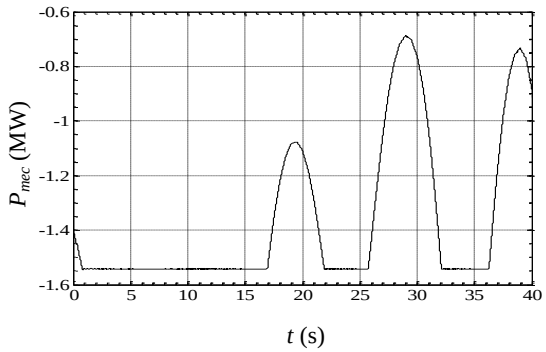

Fig. 10. Wind generator mechanical power.

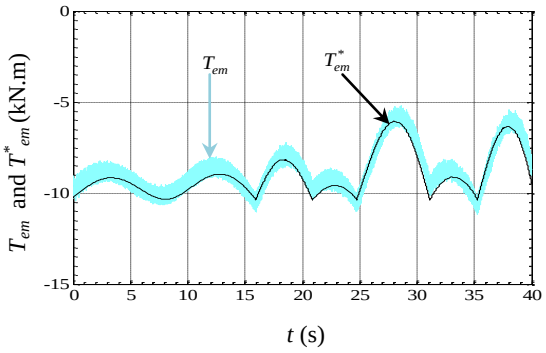

Fig. 11. Generator torque.

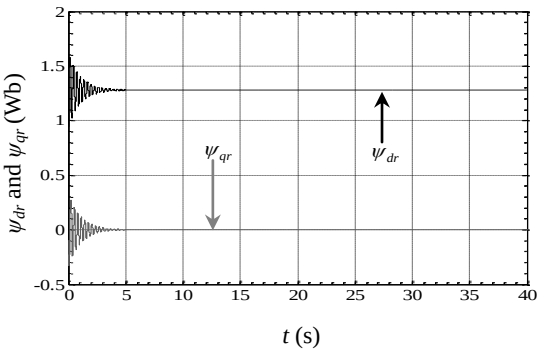

Fig. 12. Direct and quadratic rotor flux.

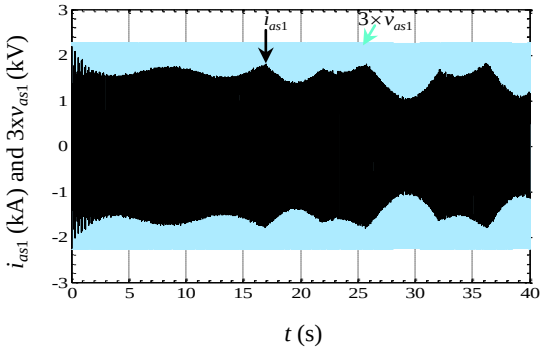

Fig. 13a. Stator current and voltage (phase as1).

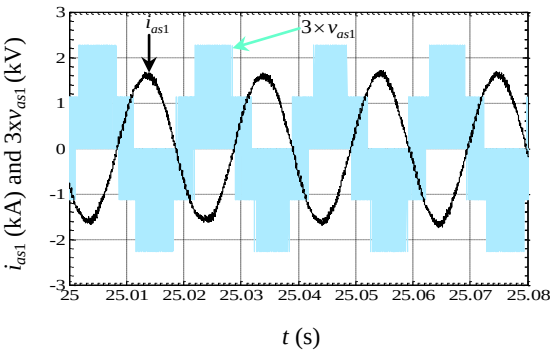

Fig. 13b. Zoom of stator current and voltage (phase as1).

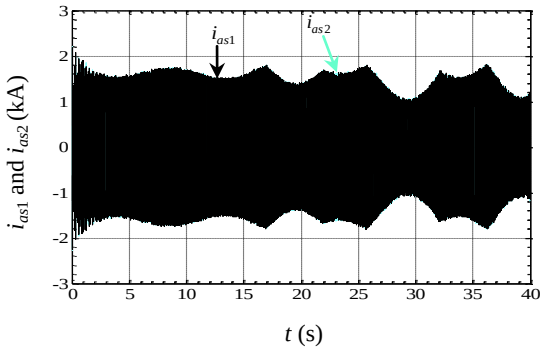

Fig. 14a. Stator currents (phase's as1 and as2).

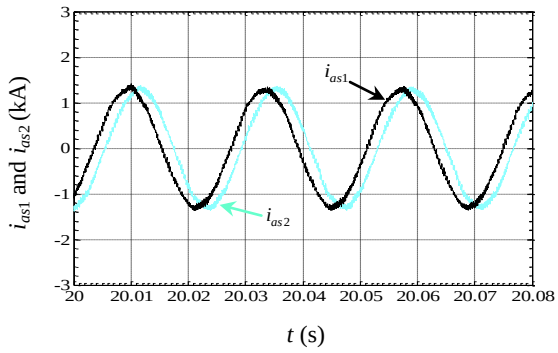

Fig. 14b. Zoom of stator currents (phase's as1 and as2).

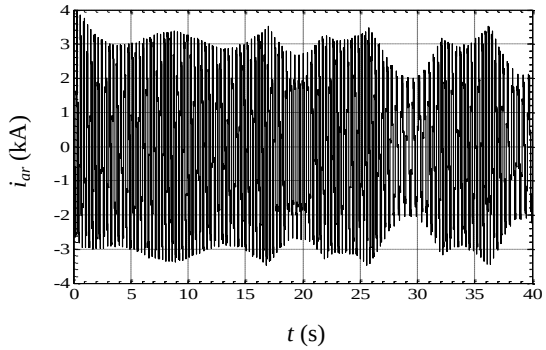

Fig. 15. Rotor current.

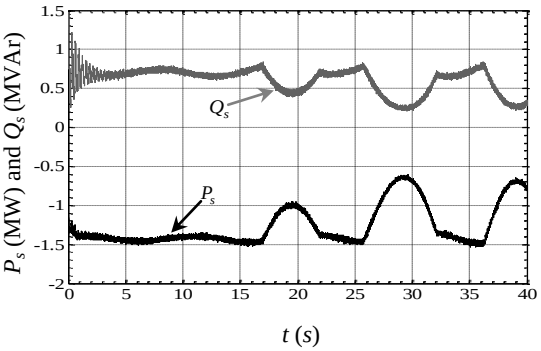

Fig. 16. Stator active and reactive powers.

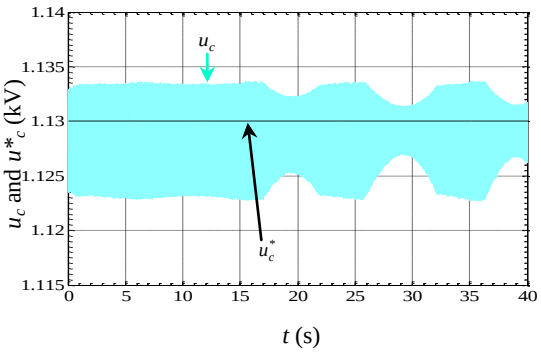

Fig. 17. DC link voltage.

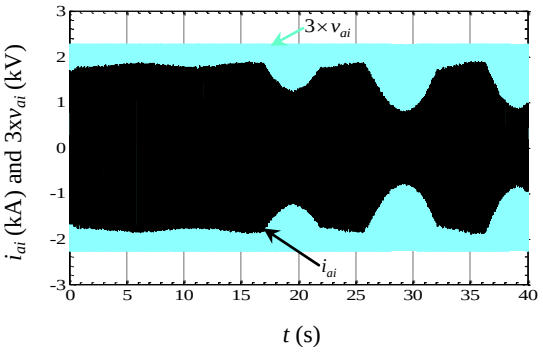

Fig. 18a. Current and voltage at the output of the inverter 3.

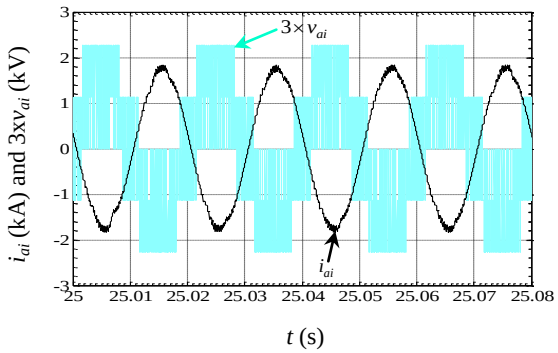

Fig. 18b. Zoom of current and voltage (inverter 3).

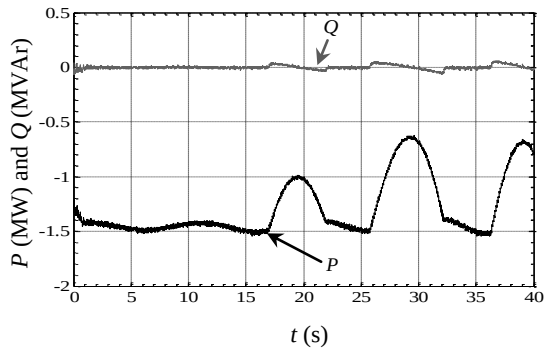

Fig. 19. Grid active and reactive powers.

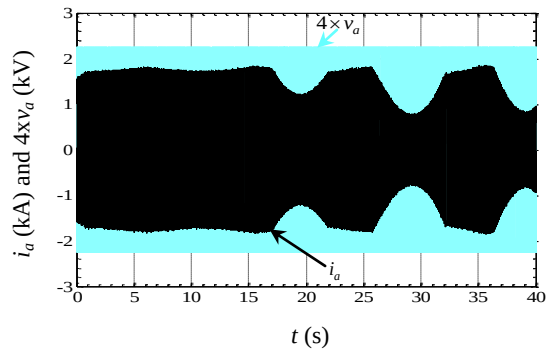

Fig. 18a. Grid current and voltage (phase a).

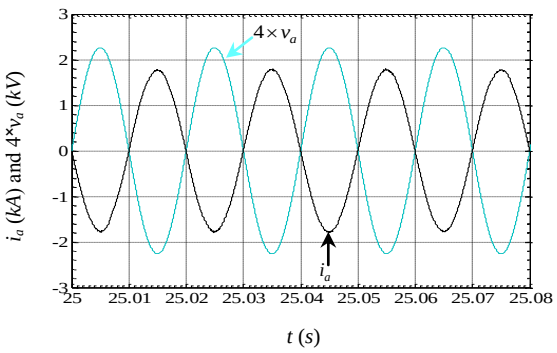

Fig. 18b. Zoom of grid current and voltage (phase a).

7. Conclusion

In this paper a fuzzy logic control associated to the indirect field oriented control of a dual-stator induction generator based wind energy conversion systems connected to the grid has been presented. A fuzzy logic control strategy was proposed to ensure stability in both operations regions and to impose the ideal feedback control solution despite model uncertainties. The proposed fuzzy speed logic controller has the advantages of robustness, fast response and good performance.

The effectiveness of the proposed controllers has been demonstrated by simulation and successfully implemented in a wind driven dual-stator induction generator system.

Appendix A. DSIM Model in *abc* reference frame

$$\begin{bmatrix}[v_{abc,1}]\\ [v_{abc,2}]\\ [v_{abc,r}]\end{bmatrix}=\begin{bmatrix}[R_{s1}][i_{abc,1}]+\frac{d}{dt}[\psi_{abc,1}]\\ [R_{s2}][i_{abc,2}]+\frac{d}{dt}[\psi_{abc,2}]\\ [R_r][i_{abc,r}]+\frac{d}{dt}[\psi_{abc,r}]\end{bmatrix}$$

With,

$[v_{abc,1}]=[v_{as1}\ \ v_{bs1}\ \ v_{cs1}]^t$,
$[v_{abc,2}]=[v_{as2}\ \ v_{bs2}\ \ v_{cs2}]^t$,
$[v_{abc,r}]=[v_{ar}\ \ v_{br}\ \ v_{cr}]^t$,
$[i_{abc,1}]=[i_{as1}\ \ i_{bs1}\ \ i_{cs1}]^t$,
$[i_{abc,2}]=[i_{as2}\ \ i_{bs2}\ \ i_{cs2}]^t$,
$[i_{abc,r}]=[i_{ar}\ \ i_{br}\ \ i_{cr}]^t$,
$[\psi_{abc,1}]=[\psi_{as1}\ \ \psi_{bs1}\ \ \psi_{cs1}]^t$,
$[\psi_{abc,2}]=[\psi_{as2}\ \ \psi_{bs2}\ \ \psi_{cs2}]^t$,
$[\psi_{abc,r}]=[\psi_{ar}\ \ \psi_{br}\ \ \psi_{cr}]^t$,
$[R_{s1}]=diag[r_{as1}\ \ r_{bs1}\ \ r_{cs1}]$,
$[R_{s2}]=diag[r_{as2}\ \ r_{bs2}\ \ r_{cs2}]$
$[R_r]=diag[r_{ar}\ \ r_{br}\ \ r_{cr}]$,
$r_{as1}=r_{bs1}=r_{cs1}=r_1$,
$r_{as2}=r_{bs2}=r_{cs2}=r_2$,
$r_{ar}=r_{bs}=r_{cs}=r_r$.

$$\begin{bmatrix}[\psi_{abc,1}]\\ [\psi_{abc,2}]\\ [\psi_{abc,r}]\end{bmatrix}=\begin{bmatrix}[L_{1,1}] & [L_{1,2}] & [L_{1,r}]\\ [L_{2,1}] & [L_{2,2}] & [L_{2,r}]\\ [L_{r,1}] & [L_{r,2}] & [L_{r,r}]\end{bmatrix}\begin{bmatrix}[i_{abc,1}]\\ [i_{abc,2}]\\ [i_{abc,r}]\end{bmatrix}$$

Where

$$[L_{1,1}]=\begin{bmatrix}L_1+L_{ms} & -\frac{L_{ms}}{2} & -\frac{L_{ms}}{2}\\ -\frac{L_{ms}}{2} & L_1+L_{ms} & -\frac{L_{ms}}{2}\\ -\frac{L_{ms}}{2} & -\frac{L_{ms}}{2} & L_1+L_{ms}\end{bmatrix},$$

$$[L_{2,2}]=\begin{bmatrix}L_2+L_{ms} & -\frac{L_{ms}}{2} & -\frac{L_{ms}}{2}\\ -\frac{L_{ms}}{2} & L_2+L_{ms} & -\frac{L_{ms}}{2}\\ -\frac{L_{ms}}{2} & -\frac{L_{ms}}{2} & L_2+L_{ms}\end{bmatrix},$$

$$[L_{r,r}]=\begin{bmatrix}L_r+L_{mr} & -\frac{L_{mr}}{2} & -\frac{L_{mr}}{2}\\ -\frac{L_{mr}}{2} & L_r+L_{mr} & -\frac{L_{mr}}{2}\\ -\frac{L_{mr}}{2} & -\frac{L_{mr}}{2} & L_r+L_{mr}\end{bmatrix},$$

$$[L_{1,2}]=\begin{bmatrix}\frac{\sqrt{3}}{2}L_{ms} & -\frac{\sqrt{3}}{2}L_{ms} & 0\\ 0 & \frac{\sqrt{3}}{2}L_{ms} & -\frac{\sqrt{3}}{2}L_{ms}\\ -\frac{\sqrt{3}}{2}L_{ms} & 0 & \frac{\sqrt{3}}{2}L_{ms}\end{bmatrix},$$

$$[L_{1,r}]=\begin{bmatrix}L_{sr} & -\frac{1}{2}L_{sr} & -\frac{1}{2}L_{sr}\\ -\frac{1}{2}L_{sr} & L_{sr} & -\frac{1}{2}L_{sr}\\ -\frac{1}{2}L_{sr} & -\frac{1}{2}L_{sr} & L_{sr}\end{bmatrix},$$

$$[L_{2,r}]=\begin{bmatrix}\frac{\sqrt{3}}{2}L_{sr} & 0 & -\frac{\sqrt{3}}{2}L_{sr}\\ -\frac{\sqrt{3}}{2}L_{sr} & \frac{\sqrt{3}}{2}L_{sr} & 0\\ 0 & -\frac{\sqrt{3}}{2}L_{sr} & \frac{\sqrt{3}}{2}L_{sr}\end{bmatrix},$$

$[L_{2,1}]=[L_{1,2}]^t$, $[L_{r,1}]=[L_{1,r}]^t$, $[L_{r,2}]=[L_{2,r}]^t$

And $L_{ms}=L_{mr}=L_{sr}=\frac{3}{2}L_m$.

Appendix B. Parameters

Turbine: Diameter = 60m, Number of Blades = 3, Hub height = 85m, Gearbox = 90.

DSIG: 1.5MW, 400V, 50Hz, 2 pole pairs, $r_1 = r_2 = 0.008\Omega$, $L_1 = L_2 = 0.134$mH, $L_m = 0.0045$H, $R_r = 0.007\Omega$, $L_r = 0.067$mH, $J = 30\text{kg.m}^2$: inertia (turbine + DSIG), $f = 2.5$N.m.s/rd: viscous coefficient (turbine+DSIG).

Appendix C. Nomenclature

Turbine

Ω_{mec}	mechanical speed of the DSIG
Ω_t	turbine speed
P_{mec_opt}	mechanical optimal
T_{aer}	aerodynamic torque
T_q	generator torque
C_P	power coefficient
λ	tip speed ratio
ρ	air density
R	turbine radius
V	wind velocity
G	gear ratio

DSIG

v_{d1}, v_{d2}, v_{q1}, v_{q2}	"*d-q*" stators voltages
i_{d1}, i_{d2}, i_{q1}, i_{q2}	"*d-q*" stators currents
ψ_{d1}, ψ_{d2}, ψ_{q1}, ψ_{q2}	"*d-q*" stators flux
v_{dr}, v_{qr}	"*d-q*" rotor voltages
i_{dr}, i_{qr}	"*d-q*" rotor currents
ψ_{dr}, ψ_{qr}	"*d-q*" rotor flux
r_1, r_2	per phase stators resistances
r_r	per phase rotor resistance
L_1, L_2	per phase stators leakages inductances
L_r	per phase rotor leakage inductance
L_m	magnetizing inductance
P	number of pole pairs
p	derivative operator
J	Inertia
f	viscous friction
T_{em}	electromagnetic torque
P_s, Q_s	Active and reactive stator powers
P, Q	Active and reactive grid powers
ω_e	speed of the synchronous reference frame
ω_r	rotor electrical angular speed
ω_{sl}	slip speed

References

1. Amimeur, H., Aouzellag, D., Abdessemed, R., Ghedamsi, K.*: Sliding mode control of a dual-stator induction generator for wind energy conversion systems.* In: International Journal of Electrical Power & Energy Systems, 42 (2012), No.1, November 2012, p. 60-70, ScienceDirect, United Kingdom.
2. Singh, G.K., *Multi-phase induction machine drive research—a Survey*. In: Electric Power Systems Research, 61 (2002), No.2, March 2002, Pages 139-147, ScienceDirect, United Kingdom.
3. Levi E.: *Recent developments in high performance variable speed multiphase induction motor drives*. In: 6th international symposium Nikola Tesla, October 18-20, 2006 Belgrade, SASA, Serbia.
4. Zhao, Y., Lipo, T.A.: *Space vector PWM control of dual three phase induction machine using vector space decomposition*. In: IEEE Transactions on Industry Applications, 31 (1995), No.5, September/ October 1995, p. 1100-1109, Piscataway, New Jersey, USA.
5. Singh, G.K., Nam, K., Lim, S.K.: *A simple indirect field-oriented control scheme for multiphase induction machine*. In: IEEE Transactions on Industrial Electronics, 52 (2005), No.4, August 2005, p. 1177-1184, Piscataway, New Jersey, USA.
6. Bojoi, R., Farina, F., Griva, G., Profumo, F., Tenconi, A.: *Direct torque control for dual three-phase induction motor drives*. In: IEEE Transactions on Industry Applications, 41 (2005), No.6, November/December 2005, p. 1627-1636, Piscataway, New Jersey, USA.
7. Amimeur, H., Abdessemed, R., Aouzellag, D., Merabet, E., Hamoudi, F.: *Modeling and analysis of dual-stator windings self-excited induction generator drives.* In: Journal of Electrical Engineering, 8 (2008), No.3, p. 18-23 [Art. 3], Timisoara, Romania.
8. Li, Y., Hu, Y., Huang, W., Liu, L., Zhang, Y.: *The capacity optimization for the static excitation controller of the dual-stator-winding induction generator operating in a wide speed range*. In: IEEE Transactions on Industrial Electronics, 56 (2009), No.2, February 2009, p. 530-541, Piscataway, New Jersey, USA.
9. Amimeur, H., Abdessemed, R., Aouzellag, D., Merabet, E., Hamoudi, F.: *A sliding mode control associated to the field oriented control of dual stator induction motor drives.* In: Journal of Electrical Engineering, 10 (2010), No.3, p. 7-13 [Art. 2], Timisoara, Romania.
10. Ameur, F., Kouzi, K.: *Optimization fuzzy speed vector control of dual stator induction generator system applied in wind power generation*. In: Journal of Electrical Engineering, 14 (2014), No.1, p. 336-343 [Art. 45], Timisoara, Romania.
11. Bu, F., Hu, Y., Huang, W., Zhuang, S., Shi, K.: *Control strategy and dynamic performance of dual stator-winding induction generator variable frequency ac generating system with inductive and capacitive loads*. In: IEEE Transactions on Power Electronics, 29 (2014), No.4, April 2014, p. 1681-1692, Piscataway, New Jersey, USA.
12. Lekhchine, S., Bahi, T., Soufi, Y.*: Indirect rotor field oriented control based on fuzzy logic controlled double star induction machine.* In: International Journal of Electrical Power & Energy Systems, 57 (2014), No.1, May 2014, p. 206-211, ScienceDirect, United Kingdom.
13. Basak, S., Chakraborty, C.: *Dual stator winding induction machine: problems, progress, and future scope*. In: IEEE Transactions on Industrial Electronics, 62 (2015), No.7, July 2015, p. 4641-4652, Piscataway, New Jersey, USA.
14. Laamayad, T., Belkacem, S.: *The stable algorithm based on a model reference adaptive control for the dual star induction machine drives*. In: Journal of Electrical Engineering, 15 (2015), No.4, p. 89-94 [Art. 13], Timisoara, Romania.
15. Tir, Z., Malik, O.P., Eltamaly, A.M.*: Fuzzy logic based speed controlof indirect rotor field oriented controlled double star induction motors connected in parallel to a single six-phase inverter supply.* In: Electric Power Systems Research, 134 (2016), January 2016, p. 126-133, ScienceDirect, United Kingdom.
16. Zadeh, L.A.: *Fuzzy sets*. In: Information and Control, (1965) 8, No. 3, June 1965, p. 338-353, ScienceDirect.

17. Feng, G.: *A survey on analysis and design of model-based fuzzy control systems*. In: IEEE Transactions on Fuzzy Systems, 14 (2006), No.5, October 2006, p. 676-697, Piscataway, New Jersey, USA.
18. Ghedamsi, K., Aouzellag, D.: *Improvement of the performances for wind energy conversions systems*. In: International Journal of Electrical Power & Energy Systems, 32 (2010), No.9, November 2010, p. 936-945, ScienceDirect, United Kingdom.
19. Amimeur, H., Abdessemed, R., Aouzellag, D., Ghedamsi, K., Hamoudi, F., Chekkal, S.: *A sliding mode control for dual-stator induction motor drives fed by matrix converters*. In: Journal of Electrical Engineering, 11 (2011), No.2, p. 136-143 [Art. 21], Timisoara, Romania.
20. Amimeur, H.: *Contribution au contrôle de la machine asynchrone double étoile (Contribution to control of dual-stator induction machine)*. Ph.D. Dissertation, Faculty of Technology, Batna University, Algeria, June 2012.
21. Merabet, E., Amimeur, H., Hamoudi, F., Abdessemed, R.: *Self–tuning fuzzy logic controller for a dual star induction machine*. In: Journal of Electrical Engineering and Technology, 6 (2011), No.1, January 2011.p. 133-138, Seoul, Korea.
22. Hamrouni, N., Jraidi, M., Chérif, A.: *New control strategy for 2-stage grid-connected photovoltaic power system*. In: Renewable Energy, 33 (2008), No.10, October 2008, p. 2212-2221, ScienceDirect, United Kingdom.